
# High-Temperature Reaction Mechanism of NH<inf>3</inf>-SCR over Cu-CHA: One or Two Copper Ions?

THE JOURNAL OF PHYSICAL CHEMISTRY C
A JOURNAL OF THE AMERICAN CHEMICAL SOCIETY



pubs.acs.org/JPCC
Article

# High-Temperature Reaction Mechanism of $NH_3$-SCR over Cu-CHA: One or Two Copper Ions?

Yingxin Feng,* Ton V. W. Janssens, Peter N. R. Vennestrøm, Jonas Jansson, Magnus Skoglundh, and Henrik Grönbeck*

Cite This: J. Phys. Chem. C 2024, 128, 6689−6701
Read Online



**ABSTRACT:** Cu-exchanged chabazite (Cu-CHA) shows good performance for selective catalytic reduction of nitrogen oxides using $NH_3$ as a reducing agent ($NH_3$-SCR). The temperature dependence of the activity has a characteristic nonmonotonic behavior with a minimum in the range 300−350 °C. The minimum signals that different reaction mechanisms or active sites dominate at low and high temperatures. The low-temperature mechanism is believed to occur over a pair of mobile $[Cu(NH_3)_2]^+$ complexes, whereas the high-temperature mechanism should proceed over framework-bound Cu ions. To explore the $NH_3$-SCR reaction over framework-bound Cu ions, we use first-principles calculations combined with mean-field microkinetic simulations. We find that the reaction proceeds over a single framework-bound Cu ion and that the first step is NO and $O_2$ coadsorption. The coadsorption competes with $NH_3$ adsorption, and the $NH_3$-SCR rate is largely determined by the adsorption energy of $NH_3$. Combining the high-temperature kinetic model with our previous low-temperature model for $NH_3$-SCR over pairs of mobile $[Cu(NH_3)_2]^+$ complexes makes it possible to describe the nonmonotonic behavior of the reaction rate. The work provides a detailed mechanistic understanding of the role and transformation of different forms of Cu ions during low- and high-temperature standard SCR in Cu-CHA.

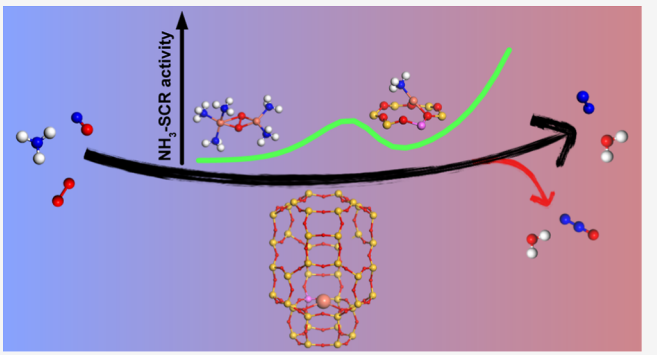




## INTRODUCTION

$NO_x$ emission control continues to be a major challenge in lean-burn engine exhaust after treatment due to increasingly stricter legislations.[1] The leading technology for $NO_x$ reduction to $N_2$ and $H_2O$ in oxygen excess is selective catalytic reduction using ammonia as the reducing agent ($NH_3$-SCR).[2] A state-of-the-art catalyst for $NH_3$-SCR is chabazite zeolite functionalized with Cu (Cu-CHA). Cu-CHA has high activity and selectivity for $NH_3$-SCR over a wide temperature range and is, moreover, hydrothermally stable at high temperatures.[2−4]

NO is the main $NO_x$-component in lean-burn engine exhausts, and $NH_3$-assisted NO reduction follows the, so-called, standard SCR-reaction, which involves an equal amount of NO and $NH_3$[2]

$$4NH_3 + 4NO + O_2 \rightarrow 4N_2 + 6H_2O \quad \text{(R1)}$$

$O_2$ is needed to accommodate the hydrogen atoms in $NH_3$. The presence of $NO_2$ has been reported to enhance or reduce the activity of Cu-CHA, dependent on reaction conditions and Cu-loading.[5,6] $O_2$ is not required for the $NH_3$-SCR reaction in the presence of $NO_2$, and the reaction can proceed according to the "fast-SCR" reaction scheme

$$2NH_3 + NO + NO_2 \rightarrow 2N_2 + 3H_2O \quad \text{(R2)}$$

The conversion of $NO_x$ over Cu-CHA under standard SCR conditions shows a nonmonotonic trend with respect to temperature, with a minimum at about 350 °C.[7,8] This minimum results in the, so-called, "seagull" profile and indicates that different reaction mechanisms dominate at low and high temperatures.[7,9−11] An additional indication that the reaction mechanism changes with temperature is different initial exponential increases of the conversion in the low- and high-temperature regimes.

The temperature dependence of the nonselective $N_2O$ formation in the $NH_3$-SCR is yet another indication that the $NH_3$-SCR reaction follows different mechanisms at low and high temperatures. $N_2O$ formation is an unwanted side reaction, which should be avoided as $N_2O$ is a potent greenhouse gas.[2] $N_2O$ formation follows the conversion of $NO_x$ at temperatures below 300 °C,[7,12] which suggests a mechanism where low-temperature $N_2O$ formation proceeds

Received: January 26, 2024
Revised: March 27, 2024
Accepted: March 28, 2024
Published: April 12, 2024

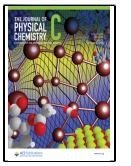





https://doi.org/10.1021/acs.jpcc.4c00554
J. Phys. Chem. C 2024, 128, 6689−6701

over Cu ions.[13,14] The $N_2O$ formation decreases and deviates from the $NO_x$ conversion above 300 °C, which indicates that the reaction mechanism changes with the temperature. The change in the $N_2O$ formation mechanism could be related to a change from a Cu-catalyzed path at low temperatures to the decomposition of ammonium nitrate, which may form under $NH_3$-SCR conditions. The decomposition of $NH_4NO_3$ is a highly activated process[13] that could result in $N_2O$ formation in the range from 250 to 350 °C.

Considerable efforts have been devoted to the understanding of the $NH_3$-SCR reaction over Cu-CHA at low temperatures.[7,15−17] X-ray absorption spectroscopy (XAS) and density functional theory (DFT) calculations have shown that Cu at low-temperature reaction conditions is solvated by $NH_3$ forming $[Cu(NH_3)_2]^+$ complexes.[18−23] The $NH_3$-SCR reaction is a redox reaction where Cu alternates between $Cu^+$ and $Cu^{2+}$. The oxidation from $Cu^+$ to $Cu^{2+}$ occurs when $O_2$ is adsorbed on a pair of $[Cu(NH_3)_2]^+$ complexes forming a $[Cu_2(NH_3)_4O_2]^{2+}$ peroxo-complex, whereas the reduction from $Cu^{2+}$ to $Cu^+$ occurs during the coupling between NO and $NH_3$ over $[Cu_2(NH_3)_4O_2]^{2+}$. The activation of $O_2$ is crucial for the $NH_3$-SCR reaction, which is strictly sequential; NO adsorbs only on $[Cu_2(NH_3)_4O_2]^{2+}$ and not on $[Cu(NH_3)_2]^+$. As $O_2$ activation at low temperatures requires two Cu ions, the mobility of $[Cu(NH_3)_2]^+$ in the zeolite is crucial.[22,23] The reaction can proceed only when two $[Cu(NH_3)_2]^+$ complexes are in the same CHA-cage. NO and $NH_3$ couple over $[Cu_2(NH_3)_4O_2]^{2+}$, forming the intermediates $H_2NNO$ and HONO, which diffuse to Brønsted acid sites where they decompose into $N_2$ and $H_2O$ with low barriers.[21] $H_2NNO$ has been suggested to decompose also over a $[Cu_2(NH_3)_4OOH]^{2+}$ complex, generating $N_2O$ and $H_2O$.[13,14] The presence of HONO during $NH_3$-SCR has recently been inferred from vibrational spectroscopy.[24]

The "seagull" profile with decreasing $NO_x$ conversion between 300 and 350 °C[7,9−11] coincides with desorption of $NH_3$ from the $[Cu(NH_3)_2]^+$ complexes as measured in temperature-programmed desorption (TPD) experiments.[14,25] This indicates that the high-temperature $NH_3$-SCR reaction proceeds over framework-bound Cu. Additionally, XAS measurements[12,26,27] and DFT-based phase diagrams[22,28] suggest that framework-bound Cu dominates the distribution of Cu ions at high temperatures.

The understanding of the reaction path at high temperatures is not as developed as that for low temperatures. Moreover, the underlying reason for the "seagull" profile in the activity is not established, and it is not clear whether the reaction at high temperatures proceeds over one or two Cu ions.[29] Gao et al.[16] measured the SCR rate and found it to change from a quadratic dependence on Cu-loading at low temperatures (200 °C) to a linear dependence at high temperatures (380 °C). The change in the dependence of Cu-loading suggests that the reaction proceeds over a pair of Cu ions at low temperatures and isolated single Cu ions at high temperatures. A low-temperature reaction mechanism over single Cu ions was proposed by Janssens et al.[30] The reaction cycle in ref 30 included NO and $O_2$ coadsorption on $Z[Cu]^+$ forming $Z[Cu(NO_3^-)]^+$ (where Z represents the anionic Al-site in the zeolite framework). $Z[Cu(NO_3^-)]^+$ was proposed to react with NO forming two $NO_2$. One $NO_2$ reacted thereafter with $NH_3$ forming $N_2$, $H_2O$, and $Z[CuOH]^+$. NO and $NH_3$ were in a subsequent step coadsorbing on $Z[CuOH]^+$ forming $N_2$ and two $H_2O$, which completed the reaction cycle. The main reaction cycle was paralleled by a cycle following the fast-SCR reaction scheme including one of the formed $NO_2$. DFT calculations were used in ref 30 to explore the proposed reaction cycle, and barriers were evaluated for the $Z[Cu(NO_3^-)]^+$ formation step and for the formation of two $NO_2$ from the reaction between $Z[Cu(NO_3^-)]^+$ and NO.

Depending on the preparation and dehydration conditions, the framework-bound Cu may be present in different forms and placed at different locations in zeolite. CHA consists of tetrahedral $TO_4$ units, where T is either silicon or aluminum arranged in 4-, 6-, and 8-membered rings, forming large and small cages.[31] High-energy-resolution fluorescence-detected X-ray absorption near-edge structure measurements[32] indicate that framework-bound Cu ions mainly are located in the 6- and 8-membered rings, forming $Z[CuOH]^+$, $ZCu^+$, or $Z_2Cu^{2+}$. The dominating form depends on the reaction conditions as well as the Cu/Al and Si/Al ratios.[27,32] As the SCR-reaction includes an oxidation step, $Z[CuOH]^+$ and $ZCu^+$ could, in principle, be parts of the reaction cycle, whereas $Z_2Cu^{2+}$ needs to be converted to $Z[CuOH]^+$ and/or $ZCu^+$ before it can participate in the reaction cycle. The mechanism for the conversion of $Z_2Cu^{2+}$ to $Z[CuOH]^+$ and $ZCu^+$ is still an open issue.[22]

In the present work, we target the reaction mechanism of high-temperature $NH_3$-SCR over Cu-CHA using DFT-based mean-field microkinetic modeling and conversion measurements. The $NH_3$-SCR reaction landscape is explored for framework-bound Cu using either one or two Cu ions. By comparison to experiments, we find that the reaction mainly proceeds over a single $Cu^+$ ion and that the reaction is limited by $NH_3$ self-poisoning. The conversion of $Z_2Cu^{2+}$ and $Z[CuOH]^+$ into $ZCu^+$ is found to be facile under the reaction conditions. We do not find any obvious path for $N_2O$ formation over framework-bound Cu ions, which is consistent with the measured absence of any correlation between Cu-loading and $N_2O$ formation at high temperatures. By combining the kinetic model for high-temperature $NH_3$-SCR with our previous model for low-temperature activity,[14] we are able to reproduce the experimentally measured "seagull" profile using the detailed first-principles reaction landscapes. We find that the minimum in activity at intermediate temperatures originates from (i) low reactant coverages in the low-temperature reaction mechanism and (ii) $NH_3$ poisoning in the high-temperature reaction mechanism. Our work provides additional understanding of the dynamic Cu-CHA catalyst where the active catalytic site changes with reaction conditions.

## COMPUTATIONAL AND EXPERIMENTAL METHODS

**First-Principles Calculations.** Spin-polarized DFT calculations are performed with the Vienna Ab-initio simulation package.[33−36] The valence electrons are described with a plane wave basis set using a cutoff energy of 480 eV, and the interaction between the valence and the core electrons is described with the projector augmented wave method.[37,38] The number of valence electrons treated in the calculations is Cu(11), Si(4), Al(3), O(6), N(5), and H(1). The *k*-point sampling is restricted to the gamma point.

The gradient-corrected Perdew−Burke−Ernzerhof[39] functional, augmented with a Hubbard-U term and van der Waals corrections, is used to describe exchange−correlation effects. Calculations on enzymatic systems with known structures and a similar Cu−OO−Cu core configuration as in the $[Cu_2(NH_3)_4O_2]^{2+}$ complex indicate that a Hubbard-U term


https://doi.org/10.1021/acs.jpcc.4c00554
J. Phys. Chem. C 2024, 128, 6689−6701

for Cu 3d is needed to properly describe the Cu−O interactions in Cu-CHA catalysts.[25,40] Here, we use a U-parameter of 6 eV, which has been determined by structural comparison with $Cu_2O$.[41] In addition, Grimme-D3 corrections are applied to account for the van der Waals interactions of the molecules in the zeolite.[42,43]

The convergence criterion in the self-consistent field loop is set to $1 \times 10^{-5}$ eV, and the structures are considered to be relaxed when the force acting on each atom is less than 0.02 eV/Å. Transition state structures and activation energies are calculated using the Climbing Image Nudged Elastic Band method.[44,45] The transition state structures are confirmed by vibrational analysis using the finite difference method. All reported energies are zero-point energy-corrected.

The periodic chabazite structure is described either with the rhombohedral unit cell, which contains 12 tetrahedral Si-sites, or with the hexagonal unit cell, which contains 36 tetrahedral Si-sites. The experimentally determined lattice parameters ($\alpha = \beta = \gamma = 94.2°$, $a = b = c = 9.42$ Å for the rhombohedral unit cell) are used and fixed during the structural optimizations. To model Cu-exchanged CHA, one or two Si atoms in the 6-membered ring of the zeolite cages are replaced by Al, yielding an Si/Al ratio of 11 or 5 for the rhombohedral unit cell. Replacing two Si atoms in the hexagonal unit cell yields a Si/Al ratio of 17. These ratios are similar to common experimental values[7,22,46] and, thus, reasonable choices when modeling the Cu-CHA material for $NH_3$-SCR.

**Microkinetic Modeling.** Mean-field microkinetic modeling is used to explore the consequences of the first-principles reaction landscapes and facilitate comparison to experiments. The steady-state reaction rates and coverages are in the mean-field approach obtained by numerically solving a set of coupled ordinary differential equations

$$\frac{\mathrm{d}\theta_i}{\mathrm{d}t} = \sum_j r_j(\vec{\theta}) c_{ji} \tag{1}$$

where each intermediate $i$ has a fractional coverage $\theta_i$. $r_j$ is the net rate constant of reaction $j$, which depends on the fractional coverages of the intermediates ($\vec{\theta}$). $c_{ji}$ reflects the stoichiometric number in reaction $j$. Each fractional coverage represents one intermediate in the catalytic cycles, and the sum of all possible intermediates is 1. MATLAB with the ode23s solver is used to numerically integrate the set of differential equations, and the equations are integrated until a steady state is reached.

According to the transition state theory (TST), the rate constant ($k^{\mathrm{TST}}$) of each elementary step is related to the change in entropy and enthalpy between the initial and transition states[47]

$$\begin{aligned} k^{\mathrm{TST}} &= \frac{k_\mathrm{B}T}{h} e^{-\Delta G^{\ddagger}/k_\mathrm{B}T} \\ &= \frac{k_\mathrm{B}T}{h} e^{\Delta S^{\ddagger}/k_\mathrm{B}} e^{-\Delta H^{\ddagger}/k_\mathrm{B}T} \\ &\approx \frac{k_\mathrm{B}T}{h} e^{\Delta S^{\ddagger}/k_\mathrm{B}} e^{-\Delta E^{\ddagger}/k_\mathrm{B}T} \end{aligned} \tag{2}$$

where $k_\mathrm{B}$ is Boltzmann's constant, $T$ is the temperature, and $h$ is Planck's constant. The $\Delta G^{\ddagger}$ is the difference in Gibbs free energy between the initial and transition states. $\Delta S^{\ddagger}$ and $\Delta H^{\ddagger}$ are the corresponding differences in entropy and enthalpy, respectively. Because the volume and pressure do not change in the reaction, the change in enthalpy ($\Delta H^{\ddagger}$) is replaced with the change in energy ($\Delta E^{\ddagger}$). The adsorption steps are considered to be nonactivated and the free energy barriers are, therefore, completely determined by entropy effects. The entropy changes in the reaction are calculated using different methods depending on the state of the reactants. The entropies for the gas phase molecules are calculated from the translational, rotational, and vibrational partition functions. For adsorbed molecules, only the vibrational partition function is used, and the translations and rotations are described as frustrated vibrations. The vibrational modes are evaluated in the harmonic approximation.[14,48]

With the rate constants from transition state theory, the net rate of each elementary step is given by

$$r_j = k_j^{+} \prod_{\mathrm{f}} \theta_{\mathrm{f}} - k_j^{-} \prod_{\mathrm{b}} \theta_{\mathrm{b}} \tag{3}$$

For the reaction steps, $j$, f, and b refer to the forward and backward reaction steps, respectively. The turnover frequency (TOF) of NO is obtained by summing the elementary steps that consume NO and is reported per Cu ion and second.

To describe the reaction rate over the entire temperature range, we combine the mechanisms for low and high temperatures using the temperature-dependent equilibrium distribution of the Cu species. Considering mobile $[Cu(NH_3)_2]^+$ and framework-bound $Z[Cu{-}NH_3]^+$, the probability that the reaction proceeds via the low-temperature mechanism [$P$(LT)] is given by

$$P(\mathrm{LT}) = \frac{1}{1 + e^{-\Delta G/k_\mathrm{B}T}} \tag{4}$$

$\Delta G$ is the Gibbs free energy difference at a specified $NH_3$ pressure between $[Cu(NH_3)_2]^+$ and $Z[Cu{-}NH_3]^+$ with one $NH_3$ molecule in the gas phase. The probability of the high-temperature mechanism [$P$(HT)] is given by $1 - P$(LT). The kinetics of the high-temperature path is the same for $Z[Cu{-}NH_3]^+$ and $ZCu^+$ as both are included in the reaction cycle (see below). The TOF of $NH_3$-SCR in the entire temperature interval ($\mathrm{TOF_{total}}$) is thus given by

$$\mathrm{TOF_{total}} = \mathrm{TOF_{LT}} \times P(\mathrm{LT}) + \mathrm{TOF_{HT}} \times P(\mathrm{HT}) \tag{5}$$

where $\mathrm{TOF_{LT}}$ and $\mathrm{TOF_{HT}}$ are the turnover frequencies at low and high temperatures, respectively.

**Measurement of $NH_3$-SCR Activity.** A Cu-CHA catalyst is prepared with a Si/Al ratio of 6.7, a Cu/Al ratio of 0.06 (1 wt % CuO), and a sieve fraction of 150−300 $\mu$m to measure the $NH_3$-SCR activity. The Cu exchange is complete as demonstrated by electron paramagnetic resonance measurements.[49] A 10 mg powder sample is diluted with 150 mg of SiC (40−60 mesh) and placed in a quartz U-tube reactor with an inner diameter of 4 mm. A Gasmet CX4000 FTIR spectrometer is connected to the reactor exit to monitor the concentrations of NO, $NO_2$, and $N_2O$ in the gas leaving the reactor in real time; the feed concentrations are determined by bypassing the reactor using a four-way valve. Prior to the measurement, the catalyst is degreened by heating to 550 °C for 30 min in 10% $O_2$. After the pretreatment, the feed gas is admitted to the reactor, and the concentration of the gas exiting the reactor is determined. The catalyst is, thereafter, cooled stepwise to preselected temperatures and kept for 30 min at each temperature to allow for stabilization and measurement of the gas composition. The gas composition is determined as the median of the measured values over the last



https://doi.org/10.1021/acs.jpcc.4c00554
J. Phys. Chem. C 2024, 128, 6689−6701

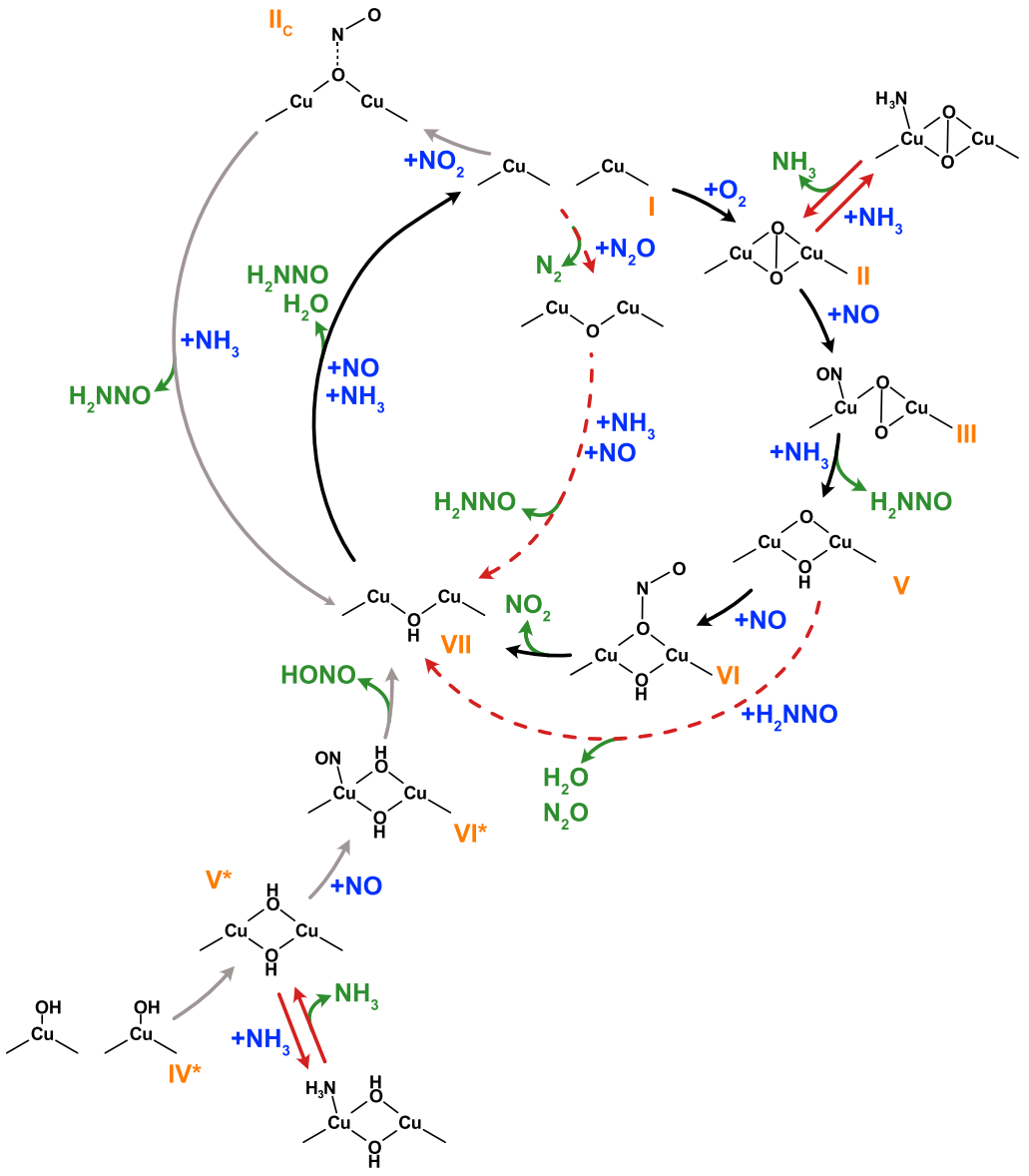


**Figure 1.** Proposed reaction cycle for high-temperature $NH_3$-SCR over two framework-bound Cu ions.

3 min at each step. To determine the TOF, we first evaluate the $NH_3$-SCR rate constant ($Cu^{-1}$ $s^{-1}$) from an integral analysis of the reactor data, assuming a plug flow reactor and a first-order reaction in NO.[14,50] Because the reaction order for $NH_3$ is close to 0,[15,50] and $O_2$ is present in excess, the overall kinetics of the $NH_3$-SCR reaction becomes first order in NO. The TOF is, thereafter, obtained by multiplication of the rate constant by the concentration of NO in the feed such that the TOF is obtained for the rate at 0% conversion. The feed gas used in the activity measurement consists of 500 ppm of NO, 600 ppm of $NH_3$, 5% $H_2O$, and 10% $O_2$ in $N_2$, at a flow of 225 N mL/min.

## RESULTS AND DISCUSSION

Previous $NH_3$-TPD[14] and XAS studies[26] show that $NH_3$ starts to desorb from the $[Cu(NH_3)_2]^+$ complex above ~250 °C, forming framework-bound $Z[Cu{-}NH_3]^+$ and eventually $ZCu^+$ at higher temperatures.[17,27,51,52] The phase diagram for $Cu^+$ ions in CHA in the presence of $NH_3$ shows that the dominant Cu species changes from $[Cu(NH_3)_2]^+$ to $Z[Cu{-}NH_3]^+$ at ~280 °C in an $NH_3$ pressure of 600 ppm (see the Supporting Information). Here, we investigate reaction mechanisms for the $NH_3$-SCR reaction in the high-temperature regime, where Cu ions preferably are bound to the zeolite framework.

The formation of $[Cu(NH_3)_2]^+$ pairs is essential in low-temperature $NH_3$-SCR, allowing for $O_2$ activation,[14,20,28] which is a key step in the sequential reaction mechanism. Assuming that two Cu ions are relevant also in the high-temperature regime, we explore first the reaction path for $NH_3$-SCR over two framework-bound Cu ions. We will, thereafter, consider the reaction over one framework-bound Cu ion.

**Reaction Cycle over Two Framework-Bound Cu Ions.** NO does not adsorb on $Cu^+$ ions at low temperatures,[28] which makes $O_2$ adsorption the first step in the reaction cycle. Considering $O_2$ adsorption on a pair of $ZCu^+$ ions, the distance between the ions should be long enough to allow for a peroxo-like framework structure. We do not obtain a peroxo-like structure when placing the two $ZCu^+$ ions in the same 6-membered ring. $O_2$ can instead adsorb in a peroxo-like $Z_2[CuOOCu]^{2+}$ structure when the pair of $ZCu^+$ ions are


https://doi.org/10.1021/acs.jpcc.4c00554
J. Phys. Chem. C 2024, 128, 6689−6701

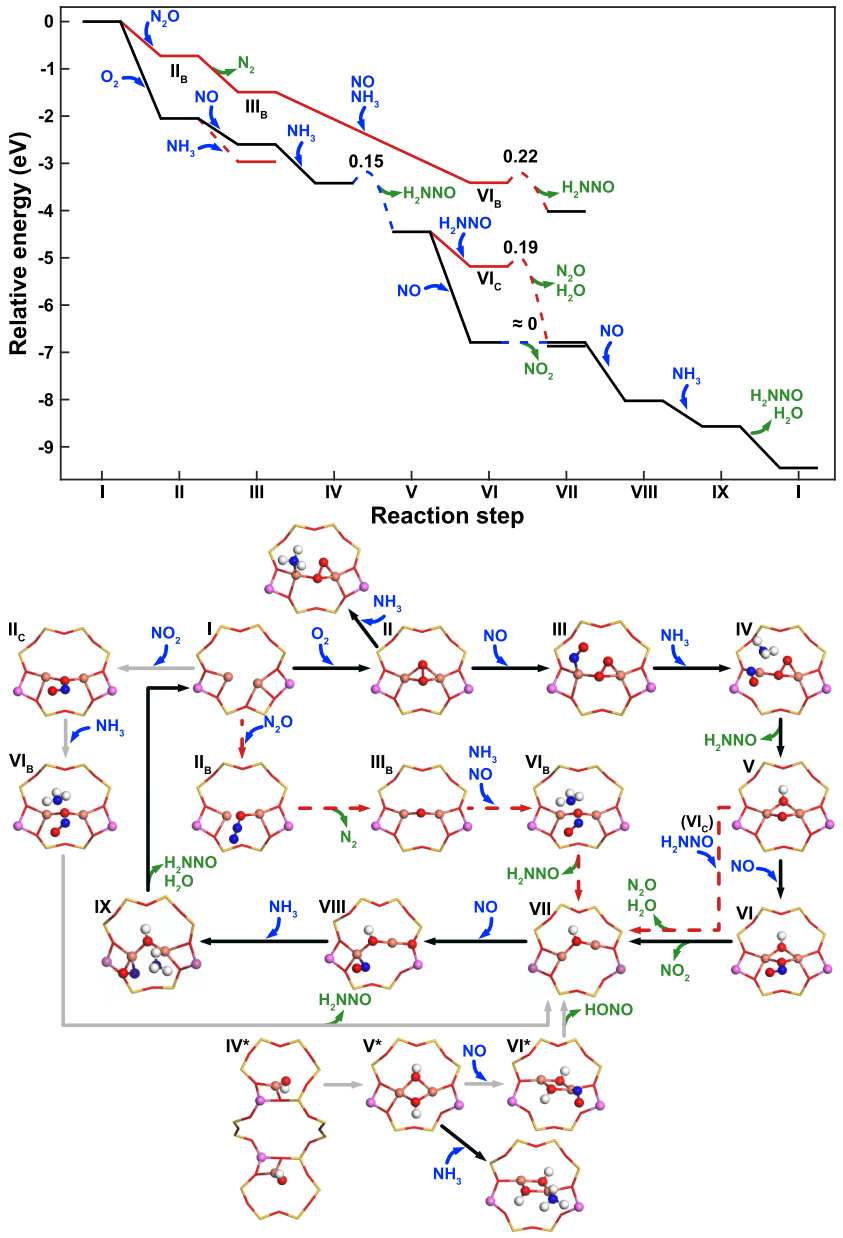


**Figure 2.** Energy landscape for high-temperature $NH_3$-SCR over two framework-bound Cu ions. Structural models of each involved intermediate are shown below the energy landscape. Atomic color code: Cu (bronze), Si (yellow), Al (pink), O (red), N (blue), and H (white).

placed in an 8-membered ring. The reaction cycle and corresponding reaction landscape are shown in Figures 1 and 2, respectively. In the considered configuration, the Al-sites are separated by two (four) Si-atoms. The adsorption energy of $O_2$ with the Al-sites separated by three Si-atoms is close to the considered structure (within 0.04 eV). NO adsorbs on $Z_2[CuOOCu]^{2+}$ with an adsorption energy of 0.54 eV. Adsorption on the $Cu^{2+}$ site is preferred over adsorption on an O-site by 0.1 eV. $NH_3$ couples with NO over the Cu-site to form $H_2NNO$, which decomposes over a Brønsted acid site to $H_2O$ and $N_2$. NO adsorbs on the O-site of $Z_2[CuOOHCu]^{2+}$ (V) forming $NO_2$ and $Z_2[CuOHCu]^{2+}$ (VII). NO does not adsorb on the Cu-sites at this stage in the reaction cycle. Adsorption of NO and $NH_3$ on $Z_2[CuOHCu]^{2+}$ results in the formation of $H_2O$ and $H_2NNO$, which decomposes to $N_2$ and $H_2O$ over the Brønsted acid sites, concluding the reaction cycle. NO adsorption on intermediate V competes with $H_2NNO$ adsorption and subsequent $N_2O$ formation, which is associated with a low barrier of 0.19 eV. The barrier for $N_2O$ formation is lower than the barrier for $H_2NNO$ diffusion through an 8-membered ring, which is about 0.3 eV.[14]

An alternative possibility in the presence of two $ZCu^+$ ions and $N_2O$ is the decomposition of $N_2O$, which is calculated to be barrierless, forming structure $III_B$. Structure $III_B$ can easily be converted to structure VII via the formation of $H_2NNO$. With two $ZCu^+$ ions, it is also possible to adsorb $NO_2$, which reacts with $NH_3$, forming $H_2NNO$ and structure VII.

The resting state of the catalyst is generally assumed to be $Z[CuOH]^+$ or $Z_2Cu^{2+}$, and here we consider how the reaction cycle can be entered from two $Z[CuOH]^+$ (structure IV*). (The conversion of $Z_2Cu^{2+}$ to $Z[CuOH]^+$ is discussed below.) In the initial state, two $Z[CuOH]^+$ are located in two 6-membered rings, which are separated by an 8-membered ring. With a small barrier of about 0.4 eV, two $Z[CuOH]^+$ combine



https://doi.org/10.1021/acs.jpcc.4c00554
J. Phys. Chem. C 2024, 128, 6689−6701

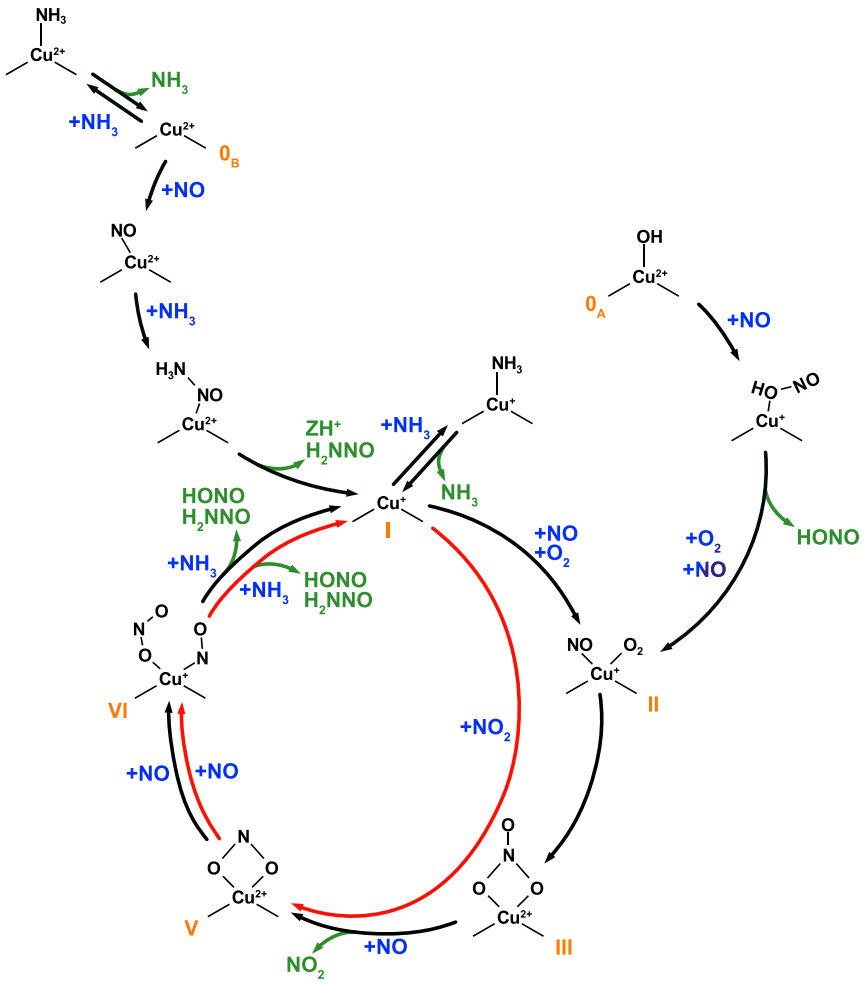


**Figure 3.** Proposed reaction cycle for high-temperature $NH_3$-SCR over one framework-bound Cu ion.

to $Z_2[CuHOOHCu]^{2+}$ in the 8-membered ring. NO can react with one OH-group, forming HONO and intermediate VII, which is a part of the main reaction cycle. Thus, the reaction can, in principle, be initialized either from $Z[CuOH]^+$ or $Z_2Cu^{2+}$ (see below).

Although the energy landscape over two Cu ions is flat with low barriers, the reaction is not necessarily fast as it requires two $ZCu^+$ located in the same 8-membered ring. The pairing of two Cu ions in the same 8-membered ring is endothermic by 1.17 eV, with respect to a configuration with the Cu ions located in different 6-membered rings. This suggests that Cu pairing is unlikely, which would slow the activation of $O_2$ slow. We stress that our results do not contradict previous measurements showing that $O_2$ can be adsorbed and activated over a pair of framework-bound $ZCu^+$ ions,[53] as these measurements were performed under $O_2$ exposure only. Under $NH_3$-SCR conditions, the adsorption energy of $NH_3$ on the $ZCu^+$ ion is higher than that for $O_2$, which means that $NH_3$ instead of $O_2$ will occupy the $ZCu^+$ species. Formation of $Z[Cu{-}NH_3]^+$ is expected to facilitate the migration of the Cu ions to separate 6-membered rings and therefore reduce the probability of Cu-pair formation.

An additional indication that Cu ion pairs are not dominating the SCR reaction at high temperatures is that only a limited amount of $N_2O$ has been measured to form above 350 °C.[54,55] The cycle in Figure 1 predicts facile $N_2O$ formation unless each formed $N_2O$ is decomposed over the catalyst. The calculated barrier for $N_2O$ decomposition is negligible, and the reaction is exothermic by −1.49 eV. Thus, the presence of $ZCu^+$ pairs could be tested by exposing the catalyst to $N_2O$ and measuring the decomposition. We have performed such experiments, where the catalyst was prepared with $ZCu^+$ and exposed to $N_2O$, see the Supporting Information. We do not observe any $N_2O$ decomposition, which indicates that pairs of framework-bound $ZCu^+$, if present, are minority species and do not affect the reaction. Consequently, as pairs of $ZCu^+$ in the Cu-CHA catalyst appear to be minority species, the most likely mechanism for $NH_3$-SCR at high temperatures involves single Cu ion sites.

**Reaction Cycle over a Single Framework-Bound Cu Ion.** The inconsistency between the SCR-reaction path over two Cu ions and the experimental data for $N_2O$ decomposition (see the Supporting Information) motivated us to investigate the SCR-reaction over one framework-bound Cu ion. The starting points for the analysis are $Z[CuOH]^+$ and $Z_2Cu^{2+}$ because these configurations generally are assumed to be present in Cu-CHA in the absence of $NH_3$.[27,32,56] The reaction cycle is shown in Figure 3 with the corresponding energy landscape in Figure 4.

Considering $Z[CuOH]^+$ at SCR conditions, NO reacts exothermically with OH, forming HONO. The reaction changes the oxidation state of the Cu ion from $Cu^{2+}$ to $Cu^+$. The formed HONO on $ZCu^+$ has a desorption energy of 0.88 eV. The desorption energy is reduced to 0.38 eV by the


https://doi.org/10.1021/acs.jpcc.4c00554
J. Phys. Chem. C 2024, 128, 6689−6701

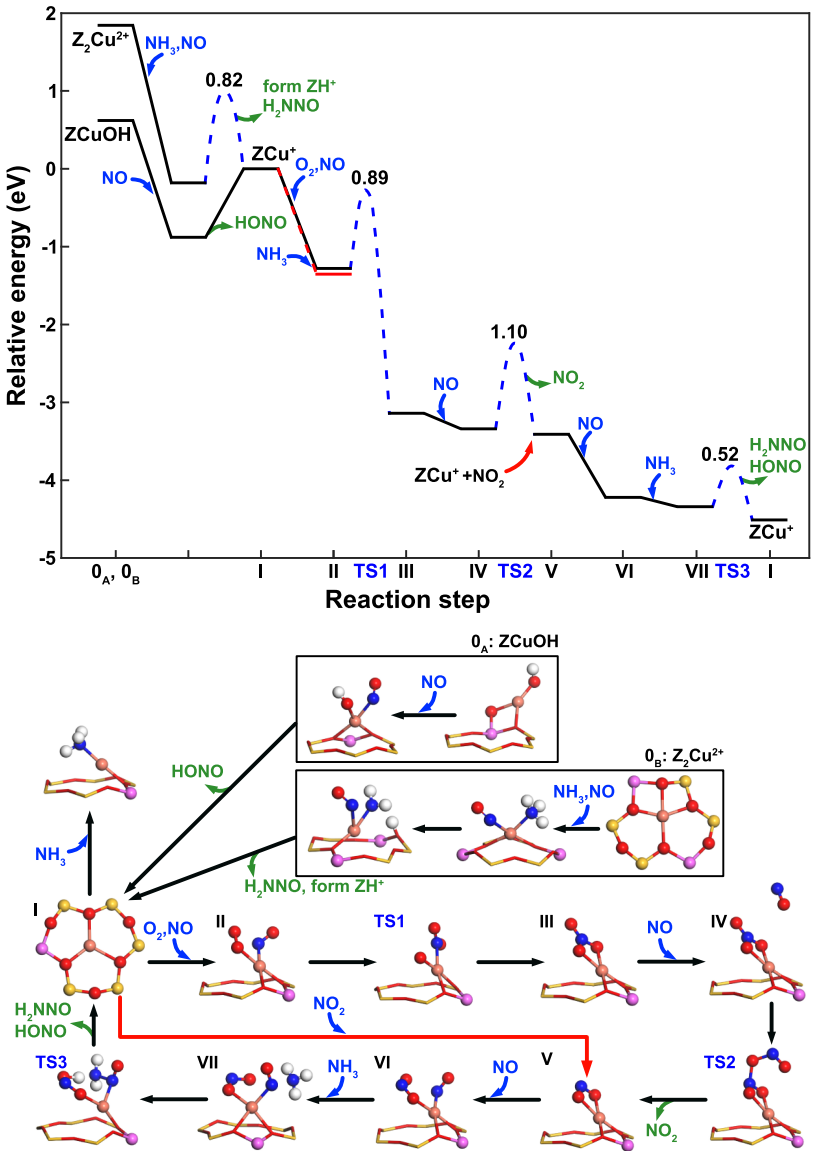


**Figure 4.** Energy landscape for high-temperature $NH_3$-SCR over one framework-bound Cu ion. The energies are referred to the $ZCu^+$ state. Structural models of each involved intermediate are shown below the energy landscape. Atomic color code as in Figure 1.

adsorption of an additional NO molecule, which results in $Z[CuNO]^+$ onto which $O_2$ adsorbs, following the main reaction cycle. Based on DFT-calculations, Liu et al.[57] proposed that adsorbed $NO_2$ facilitates HONO desorption, which is similar to our results with NO. However, as our mechanism focuses on the reaction at high temperatures, HONO desorption will not limit the reaction kinetics; thus, the coadsorb NO intermediate is not included in the present mechanism.

$Z_2Cu^{2+}$ is converted to a framework-bound $Cu^+$ ion and a Brønsted acid site by coupling of NO and $NH_3$ over $Z_2Cu^{2+}$ forming $H_2NNO$ while a proton from $NH_3$ is transferred to the Al−O−Si site. The reaction changes the oxidation state of the Cu ion from $Cu^{2+}$ to $Cu^+$, and $Z_2Cu^{2+}$ is connected in this way to the main reaction cycle. The reaction is endothermic by 0.18 eV and has a barrier of 0.82 eV. It has previously been suggested that $Z_2Cu^{2+}$ can be converted to $Z[CuOH]^+$ by $H_2O$ decomposition.[22] We find that water splitting over $Z_2Cu^{2+}$ is endothermic by 0.71 eV (in agreement with the calculations by Paolucci et al.[22]) and associated with a barrier of 1.24 eV. Based on DFT calculations, the conversion of $Z_2Cu^{2+}$ to framework-bound $Cu^+$ has previously been suggested to occur via mobile $[Cu(NH_3)_4]^{2+}$ species.[58] As $[Cu(NH_3)_4]^{2+}$ species are estimated to decompose above 230 °C,[22] we anticipate that the $NH_3$-SCR path for $Z_2Cu^{2+}$ conversion to framework-bound $Cu^+$ in Figure 3 should dominate at high temperatures.

Knowing that $ZCu^+$ can be formed from $Z[CuOH]^+$ and $Z_2Cu^{2+}$ during reaction conditions, we investigate the $NH_3$-SCR reaction over $ZCu^+$. The first step in the cycle is adsorption of $O_2$ and NO. The adsorption energy of $O_2$ is 0.37 eV, whereas the adsorption energy of NO is 0.90 eV. The combined adsorption energy is close to additive as the adsorption energy of $O_2$ and NO on the $ZCu^+$ is calculated to be 1.27 eV. $O_2$ reacts with a barrier of 0.89 eV to form $Z[Cu(NO_3^-)]^+$, where the oxidation state of Cu changes from $Cu^+$ to $Cu^{2+}$. The formation of adsorbed $NO_3^-$ is exothermic by 1.86 eV. The formation of $Z[Cu(NO_3^-)]^+$ was calculated in ref 30 to have a barrier of 1.08 eV. NO reacts with the adsorbed $NO_3^-$ to form $Z[Cu(NO_2^-)]^+$ and nonadsorbed $NO_2$ with a barrier of 1.10 eV. A similar reaction step has been reported in


https://doi.org/10.1021/acs.jpcc.4c00554
J. Phys. Chem. C 2024, 128, 6689−6701

Table 1. Energy ($\Delta E^{\ddagger}$) and Entropy ($\Delta S^{\ddagger}$) Contributions to the Reaction Barriers of the Considered Elementary Steps[a]

| no. | elementary step | $\Delta E_f^{\ddagger}$ | $\Delta E_b^{\ddagger}$ | $\Delta S_f^{\ddagger}$ | $\Delta S_b^{\ddagger}$ |
|---|---|---|---|---|---|
| r1 | $NO + * \overset{r1}{\leftrightarrow} NO^{-} *$ | 0.00 | 0.90 | −108.0 | 0 |
| rb | $NH_3 + * \overset{rb}{\leftrightarrow} NH_3^{-} *$ | 0.00 | 1.35 | −108.6 | 0 |
| r2 | $O_2 + NO^{-} * \overset{r2}{\leftrightarrow} O_2^{-}NO^{-} *$ | 0.00 | 0.37 | −111.3 | 0.0 |
| r3 | $O_2^{-}NO^{-} * \overset{r3}{\leftrightarrow} NO_3^{-} *$ | 0.89 | 2.75 | −9.16 | 19.14 |
| $r4_{phys}$ | $NO + NO_3^{-} * \overset{r4_{phys}}{\longleftrightarrow} NO\cdots NO_3^{-} *$ | 0.00 | 0.12 | −88.2 | 0.0 |
| r4 | $NO\cdots NO_3^{-} * \overset{r4}{\leftrightarrow} NO_2^{-} * + NO_2\cdots *$ | 1.10 | 1.17 | −53.1 | −66.1 |
| r5 | $NO + NO_2^{-} * \overset{r5}{\leftrightarrow} NO^{-}NO_2^{-} *$ | 0.00 | 0.81 | −12.2 | 0.0 |
| $r6_{phys}$ | $NH_3 + NO^{-}NO_2^{-} * \overset{r6_{phys}}{\longleftrightarrow} NH_3\cdots NO^{-}NO_2^{-} *$ | 0.00 | 0.14 | −91.6 | 0.0 |
| r6 | $NH_3\cdots NO^{-}NO_2^{-} * \overset{r6}{\rightarrow} * + H_2NNO + HONO *$ | 0.52 | | −59.0 | |
| r7 | $NO_2\cdots * \overset{r7}{\leftrightarrow} NO_2^{-} *$ | 0.00 | 1.35 | −128.0 | 0.0 |
| r8 | $HONO + NH_3 \overset{r8}{\rightarrow} H_2NNO + H_2O$ | 0.38 | | 19.7 | |
| r9 | $H_2NNO \overset{r9}{\rightarrow} N_2 + H_2O$ | 0.38 | | −70.1 | |

[a]Energy is given in eV and entropy in J/mol·K. The * in the elementary steps represents one $ZCu^{+}$ site.

refs 30 and 57 with a lower barrier (~0.66 eV). The difference in the barrier can originate from the choice of exchange−correlation functionals and the spin state considered during the reaction. The barrier was, in our case, calculated with a triplet configuration, which is a stable configuration. The formation of $Z[Cu(NO_2^{-})]^{+}$ is close to thermo-neutral with respect to $Z[Cu(NO_3^{-})]^{+}$. $Z[Cu(NO_2^{-})]^{+}$ reacts with NO and $NH_3$, forming HONO and $H_2NNO$ with a barrier of 0.52 eV. The formation of HONO and $H_2NNO$ is accompanied by a reduction of the Cu site from $Cu^{2+}$ to $Cu^{+}$. The reaction cycle is completed as HONO and $H_2NNO$ desorb, yielding the $ZCu^{+}$ species.

HONO and $H_2NNO$ will further react and decompose into $H_2O$ and $N_2$ over Brønsted acid sites with low barriers.[21] $NH_3$ in the HONO conversion and $H_2NNO$ decomposition originate either from the feed gas or, in the case of limited $NH_3$ supply, from $NH_3$ stored at Lewis acid sites. This picture is consistent with the transient experiments in ref 17. The proposed reaction cycle is similar to the cycle proposed in ref 30 with the overall scheme

$$2NH_3 + 3NO + O_2 \rightarrow 2N_2 + NO_2 + 3H_2O \qquad (R3)$$

$NO_2$ that is formed in the cycle adsorbs on $ZCu^{+}$, forming again $Z[Cu(NO_2^{-})]^{+}$, and follows the red inner cycle in Figure 3, which, actually, represents the fast SCR reaction scheme (R2). Assuming that $NO_2$ generated in R3 will adsorb on $ZCu^{+}$ and react, we can add the reactions R3 and R2, which results in the overall reaction equation for the standard SCR reaction (R1). Note that the reaction steps with high barriers are circumvented in the presence of $NO_2$, which potentially enhances the $NH_3$-SCR rate by following the fast-SCR reaction scheme, in agreement with the suggestion in ref 30. The effect of $NO_2$ on the reaction rate and kinetics of $NH_3$-SCR is discussed further below.

**Kinetic Model for High-Temperature $NH_3$-SCR.** To investigate the kinetic behavior of the energy landscape for the cycle with one $ZCu^{+}$, we construct a microkinetic model using the calculated energy landscape. As both $Z[CuOH]^{+}$ and $Z_2Cu^{2+}$ can be converted to $ZCu^{+}$ during reaction conditions, we focus on a catalytic cycle over $ZCu^{+}$. The considered elementary reaction steps with the corresponding enthalpy and entropy barriers are presented in Table 1. Our previous kinetic study of the low-temperature $NH_3$-SCR reaction[14] revealed that the decomposition of HONO and $H_2NNO$ over the Brønsted acid sites are facile and can be expected be fast and irreversible also at high temperatures.

The reaction cycle starts with the adsorption of NO, $O_2$, and $NH_3$, which are considered in r1, r2, and rb. We chose to have NO adsorption before the adsorption of $O_2$. However, in contrast to the low-temperature $NH_3$-SCR reaction, the order of adsorption is arbitrary because the adsorption of NO and $O_2$ is barrierless with similar changes in entropies. The adsorbed NO and $O_2$ react to form $Z[Cu(NO_3^{-})]^{+}$ (r3), which upon additional NO adsorption converts to adsorbed $NO_2^{-}$ and $NO_2$ physisorbed in the zeolite ($r4_{phys}$ and r4). Yet another NO adsorbs on $Z[Cu(NO_2^{-})]^{+}$ in r5. In $r6_{phys}$ $NH_3$ is physisorbed in the zeolite. $H_2NNO$ and HONO are formed from the reaction where the physisorbed $NH_3$ reacts with coadsorbed NO and $NO_2$ (r6). The formed HONO reacts with $NH_3$ to form $H_2NNO$ and $H_2O$ (r8). Finally, $H_2NNO$ is decomposed to $N_2$ and water (r9). Physisorbed $NO_2$ formed in r4 adsorbs on $ZCu^{+}$ in r7. The reason to include the physisorbed states for NO, $NO_2$, and $NH_3$ is that this procedure provides a convenient way to evaluate the entropy changes along the reaction. In addition, the physisorbed state of $NO_2$ is needed to account for $NO_2$ that is formed (outer cycle in Figure 3) and consumed (inner cycle in Figure 3) during the SCR-reaction.

We study the reaction kinetics under standard $NH_3$-SCR conditions at a total pressure of 1 atm, with 600 ppm of $NH_3$, 500 ppm of NO, 10% of $O_2$, and balance $N_2$. The TOF and probability of intermediates in the reaction cycle (coverages) are presented in Figure 5a,b. The high-temperature $NH_3$-SCR reaction has a light-off at about 350 °C and the TOF increases until a plateau is reached at about 500 °C. The light-off temperature is connected to the decomposition of the Z[Cu−



https://doi.org/10.1021/acs.jpcc.4c00554
J. Phys. Chem. C 2024, 128, 6689−6701

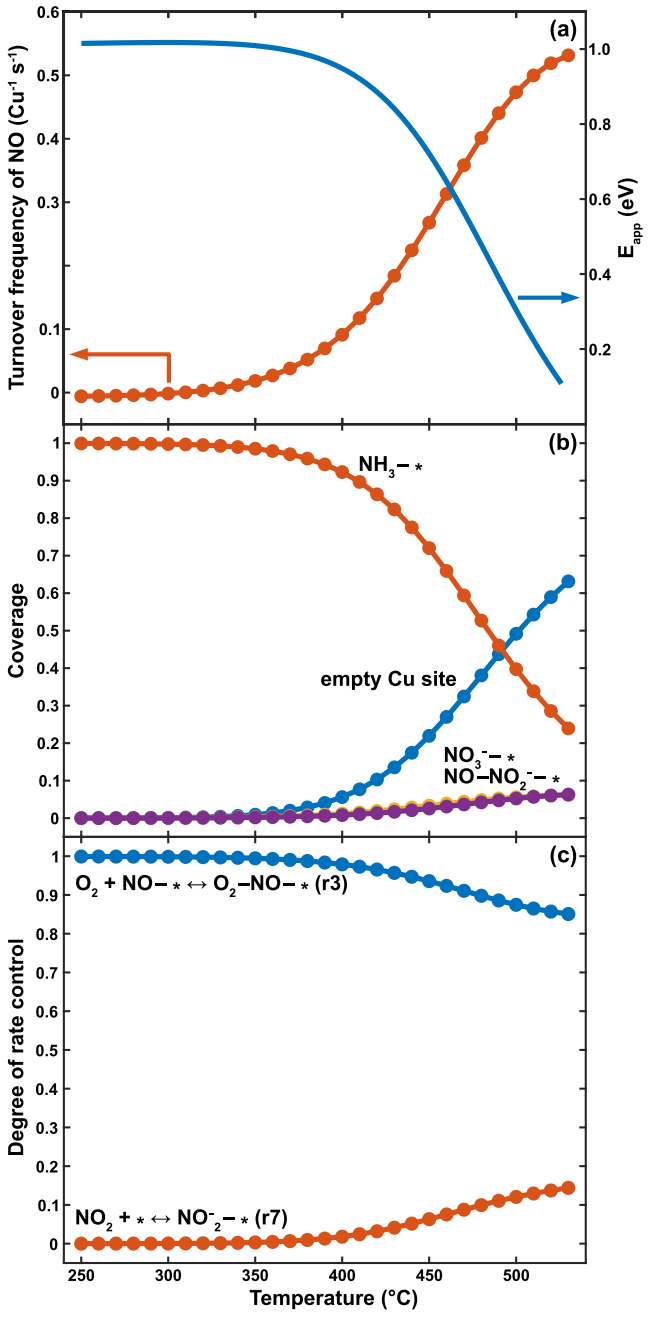


**Figure 5.** (a) Simulated TOF for NO conversion (orange) and the apparent activation energy ($E_{app}$) over Cu-CHA as a function of temperature over one framework-bound Cu ion. (b) Coverage of dominating intermediates. (c) Degree of rate control analysis. The simulation is performed with 600 ppm of $NH_3$, 500 ppm of NO, 10% $O_2$, and balance $N_2$.

$NH_3]^+$ intermediate. The calculated coverages of the intermediates reveal that almost all Cu is present as $Z[Cu–NH_3]^+$ below 350 °C. Because NO or $O_2$ cannot adsorb on this intermediate, the reaction does not proceed at low temperatures. By increasing the temperature to above 400 °C, $Z[Cu–NH_3]^+$ decomposes to $ZCu^+$. As $ZCu^+$ reacts with $O_2$ and NO, the rate of the $NH_3$-SCR reaction increases once this temperature has been reached. The coverage of $ZCu^+$ gradually increases as the temperature exceeds 400 °C, whereas the coverages of $Z[Cu(NO_3^-)]^+$ and $Z[Cu(NO–NO_2^-)]^+$ are below 0.06, making experimental detection of these intermediates challenging. Other intermediates have even lower coverages. The fractions of $Cu^+$ and $Cu^{2+}$ were analyzed by counting the number of Cu species with different oxidation states in the considered temperature range (see the Supporting Information). The analysis shows that $Cu^+$ dominates over the entire temperature interval considering only the high-temperature mechanism. Combining the low- and high-temperature mechanisms, we reproduce the experimentally observed presence of $Cu^{2+}$ at low temperatures and the switch-over to $Cu^+$ at high temperatures[8] (see the Supporting Information).

The TOF is used to calculate the temperature-dependent apparent activation energy. The apparent activation energy is 1.05 eV below 350 °C and decreases to 0.95 eV at 400 °C; see Figure 5a. We deduce an experimental apparent activation energy of 1.3 eV in the temperature range 375−420 °C from our measurements, which is in agreement with previous reports.[46]

A degree of rate control ($\chi_i$) analysis[59] is performed to understand which elementary steps control the reaction. To calculate $\chi_i$, the value of rate constants for the forward and backward reaction for each elementary step are increased by 1% while keeping the equilibrium constant ($K_i$) and the rate constants of all other reaction steps fixed

$$\chi_i = \frac{k_i}{\mathrm{TOF}}\left(\frac{\partial \mathrm{TOF}}{\partial k_i}\right)_{K_i} \tag{6}$$

The results of the degree of rate control analysis are shown in Figure 5c. Only the elementary steps that have a substantial degree of rate control are shown, namely, the formation of adsorbed NO and $O_2$ (r3) and the adsorption of $NO_2$ (r7). The analysis shows that the $NH_3$-SCR rate is controlled by r3 over the entire temperature range. The reason for r3 having rate control below 400 °C is that the adsorption of NO and $O_2$ is hindered by competitive $NH_3$ adsorption and the high barrier for $NO_3^-$ formation. The desorption energy of $NH_3$ is 1.35 eV, which is the highest barrier in the reaction landscape. Once the coverage of $ZCu^+$ increases, NO and $O_2$ can adsorb, and the reaction proceeds. The dominating degree of rate control for r3 is evident from the reaction energies. At higher temperatures, the $NO_2$ adsorption has some degree of rate control. The degree of rate control for $NO_2$ adsorption arises as $NO_2$ is produced in the outer reaction cycle in Figure 3 and reacts in the inner reaction cycle. The outer reaction cycle has an overall reaction according to R3. As r7 has some degree of rate control, not all of the $NO_2$ is converted in the reaction cycle. We note that $NO_2$ is not formed experimentally during standard SCR;[60] thus, $NO_2$ is in the experimental situation and converted over Brønsted acid sites[61] or adjacent Cu ions in the zeolite.

As the reaction cycle includes both NO and $NO_2$, it could also describe the fast SCR mechanism. We study this situation by running the kinetic model with a total pressure of 1 atm, with 600 ppm of $NH_3$, 250 ppm of NO, 250 ppm of $NO_2$, 10% of $O_2$, and balance $N_2$. In the presence of $NO_2$, reactions r3 and r4, which have high reaction barriers, can be circumvented, and the TOF of the overall reaction is considerably higher than for the standard SCR conditions. The TOF as a function of the $NO_2/(NO + NO_2)$ ratio is shown in Figure 6. The TOF over the Cu ion site has a clear maximum with equal amounts of NO and $NO_2$, which agrees with experiments.[5,62]

**Origin of the "Seagull" Profile.** In our previous work,[14] we proposed a reaction cycle for the low-temperature $NH_3$-


https://doi.org/10.1021/acs.jpcc.4c00554
J. Phys. Chem. C 2024, 128, 6689−6701

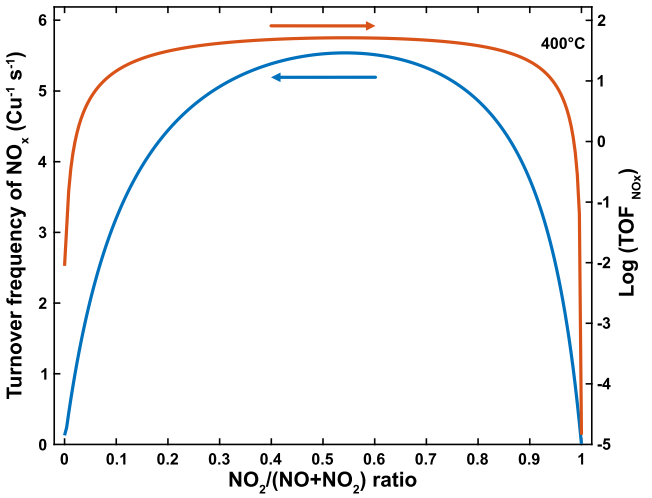


**Figure 6.** Effect of the $NO_2/(NO + NO_2)$ ratio on $NO_x$ TOF over Cu-CHA from the microkinetic model. The TOF is shown both on a linear and a logarithmic scale.

SCR, which showed good agreement with experimental apparent activation energy and reaction orders in NO, $O_2$, and $NH_3$. However, the investigated temperatures were below 250 °C where the linear $[Cu(NH_3)_2]^+$ complexes dominate. The high-temperature kinetic model proposed in this work provides atomistic insight into the reaction at high temperatures and allows us to construct a model that is valid for both low and high temperatures.

To connect the low- and high-temperature models, the probabilities that the Cu ions are in the form of $[Cu(NH_3)_2]^+$ or $Z[Cu{-}NH_3]^+$ are calculated as a function of temperature. The complete TOF is obtained by summing the weighted TOFs for the two regimes (eq 5), as shown by the dashed line in Figure 7. The total TOF has a characteristic local minimum

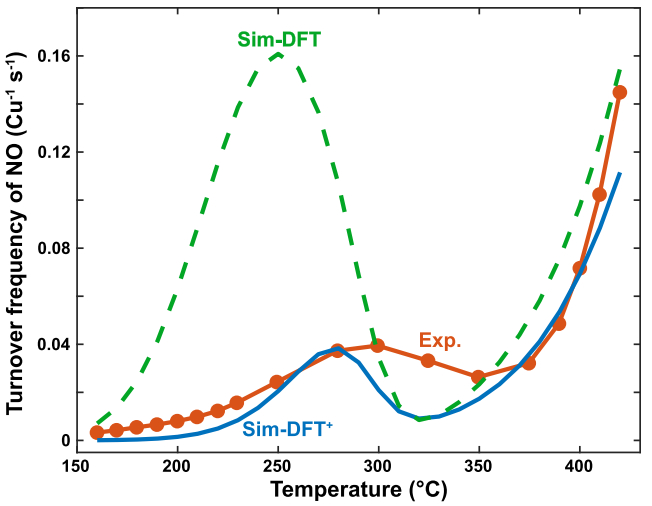


**Figure 7.** Simulated TOF from simulated low- and high-temperature $NH_3$-SCR over Cu-CHA. The dashed line (Sim-DFT) shows the results with kinetic parameters according to Table 1 and ref 14, whereas the solid line (Sim-DFT$^+$) shows the results with slightly adjusted parameters for the rate-controlling steps (see text). The simulated results are compared to experimental $NO_x$ conversion data (Exp.). The simulations and experiments are performed with 600 ppm of $NH_3$, 500 ppm of NO, 10% $O_2$, and balance $N_2$. The experiments are performed over a Cu-CHA (1 wt % CuO) sample.

at intermediate temperatures. The low-temperature behavior is characterized by a reaction onset at about 150 °C and a maximum at 250 °C. The decrease in TOF above 250 °C has two reasons: (i) Decrease in $O_2$ coverage on paired $[Cu(NH_3)_2]^+$ complexes, which is needed for the reaction to proceed along the low-temperature path. (ii) Decomposition of the $[Cu(NH_3)_2]^+$ complexes forming $Z[Cu{-}NH_3]^+$. As the high-temperature mechanism requires $ZCu^+$, the TOF according to the high-temperature mechanism is low at intermediate temperatures. It is only when the coverage of $ZCu^+$ becomes appreciable that the TOF starts to increase again. The minimum of the TOF is in the present calculations at 320 °C, which is in the temperature region where the minimum is typically observed experimentally.[8,31]

The comparison between the experimental and simulated results shows good agreement. The main differences are that (i) the simulated low-temperature maximum is shifted by 50 °C to lower temperatures and that (ii) the light-off at high-temperature is at a slightly higher temperature than the experimental TOF and with a weaker temperature dependence. It is clear that the exact shape of the simulated TOF depends sensitively on the calculated kinetic parameters. The accuracy of the calculated kinetic parameters depends on both the inherent accuracy of the applied exchange−correlation functional in the DFT calculations and the atomistic model with chosen Si/Al and Cu/Al ratios. Previous DFT calculations show that the desorption energy of $NH_3$ from $[Cu(NH_3)_x]^+$ ($x$ = 1−4) may change ∼0.3 eV between different functionals[25] and that the Al-distribution affects the stability of $[Cu(NH_3)_2]^+$ pairs.[63]

Having access to mechanistic models for the low- and high-temperature regimes and experiments, we can modify the kinetic parameters for the rate-controlling steps in the two models within reasonable margins to study whether the difference between experiments and simulations is related to the accuracy of the model (see the Supporting Information). The rate-controlling step in the low-temperature model is $NH_3$ desorption from a $[Cu_2(NH_3)_5O_2]^{2+}$ complex,[14] whereas $NH_3$ desorption from $Z[Cu{-}NH_3]^+$ is rate-controlling in the high-temperature model. Adjusting $\Delta E_b^{\ddagger}$ by 0.16 eV for the low-temperature mechanism and $\Delta S_b^{\ddagger}$ by −3 J/mol·K for the high-temperature mechanism, we obtain the solid simulated line in Figure 7. These adjustments, which are within the anticipated DFT-accuracy range, bring the simulated results in quantitative agreement with the experimental data. The remaining difference between simulated and measured results in the low-temperature regime is related to Al-distribution and the assumed probability of $[Cu(NH_3)_2]^+$ pairing.[14,20]

## CONCLUSIONS

We use first-principles DFT calculations in combination with mean-field microkinetic simulations to explore $NH_3$-SCR over Cu-CHA in the high-temperature regime. The reaction is investigated over a pair of $ZCu^+$ ions as well as a single $ZCu^+$ ion. The reaction over two $ZCu^+$ ions has a flat potential energy landscape. However, the pair of $Cu^+$ ions is not stable with respect to fragmentation into two separated $ZCu^+$ sites and the envisioned kinetic behavior, such as facile $N_2O$ decomposition, is not consistent with experimental data.

The proposed reaction cycle over one $Cu^+$ ion is composed of two intertwined catalytic cycles where the first cycle consumes three NO molecules while producing one $NO_2$ molecule and the second cycle consumes the $NO_2$ molecule


https://doi.org/10.1021/acs.jpcc.4c00554
J. Phys. Chem. C 2024, 128, 6689−6701

together with an additional NO molecule. The combined cycles follow the standard SCR reaction (R1) and the second cycle follows the stoichiometry of the fast-SCR reaction (R2). We find that $ZCu^+$ is easily formed during SCR-reaction conditions from $Z[CuOH]^+$ and $Z_2Cu^{2+}$, which commonly are present in the resting state of the catalyst. The first-principles-based kinetic model for $NH_3$-SCR over $ZCu^+$ shows that the reaction is limited by $NH_3$ self-poisoning. The reaction path does not include Cu species, where $H_2NNO$ could decompose into $N_2O$, which indicates that high-temperature $N_2O$ formation is not directly linked to the Cu-sites.

By combining the high-temperature kinetic model with our previous low-temperature model, where the reaction proceeds over a pair of mobile $[Cu(NH_3)_2]^+$ complexes, we are able to reproduce the characteristic "seagull" profile of the $NH_3$-SCR activity with a local minimum at intermediate (~300 °C) temperatures. The minimum activity has two main reasons. (i) The activity of the low-temperature mechanism starts to decrease above 250 °C due to a decreasing $O_2$ coverage on pairs of $[Cu(NH_3)_2]^+$ complexes. (ii) $[Cu(NH_3)_2]^+$ complexes decompose above 250 °C into $Z[Cu{-}NH_3]^+$, which is a poisoned state in the high-temperature mechanism. The onset of the high-temperature activity requires that $NH_3$ desorbs, allowing for NO and $O_2$ adsorption. Interestingly, at low temperatures, the onset of the reaction is also determined by $NH_3$ desorption where $NH_3$ desorbs from $[Cu_2(NH_3)_5O_2]^{2+}$, forming $[Cu_2(NH_3)_4O_2]^{2+}$ over which the reaction can proceed.

For the first time, the present work provides a consistent picture of $NH_3$-SCR over Cu-CHA over the entire relevant temperature interval. The detailed atomistic understanding stresses the dynamic behavior of the catalyst material where the function of the Cu ions depends sensitively on the reaction conditions and offers a possibility to further improve the catalytic performance of Cu-CHA for $NH_3$-SCR.

## ■ ASSOCIATED CONTENT

### Supporting Information

The Supporting Information is available free of charge at https://pubs.acs.org/doi/10.1021/acs.jpcc.4c00554.

Phase diagram for $[Cu(NH_3)_x]^+$ in CHA as a function of temperature and $NH_3$ pressure, procedure to fit kinetic parameters of rate-controlling steps to experimental data, measurement of $N_2O$ consumption over Cu-CHA, temperature-dependent fractions of $Cu^+$ and $Cu^{2+}$, atomic structures from the DFT calculations, and raw data from kinetic simulations and experiments (PDF)

Structural data (ZIP)

Kinetic data (ZIP)

## ■ AUTHOR INFORMATION


### Corresponding Authors

**Yingxin Feng** − *Department of Physics and Competence Centre for Catalysis, Chalmers University of Technology, SE-412 96 Göteborg, Sweden;* orcid.org/0000-0002-5817-4391; Email: yingxin@chalmers.se

**Henrik Grönbeck** − *Department of Physics and Competence Centre for Catalysis, Chalmers University of Technology, SE-412 96 Göteborg, Sweden;* orcid.org/0000-0002-8709-2889; Email: ghj@chalmers.se

### Authors

**Ton V. W. Janssens** − *Umicore Denmark ApS, DK-2970 Hørsholm, Denmark;* orcid.org/0000-0002-1225-0942

**Peter N. R. Vennestrøm** − *Umicore Denmark ApS, DK-2970 Hørsholm, Denmark;* orcid.org/0000-0002-6744-5640

**Jonas Jansson** − *Volvo Group Trucks Technology, SE-405 08 Göteborg, Sweden*

**Magnus Skoglundh** − *Department of Physics and Competence Centre for Catalysis, Chalmers University of Technology, SE-412 96 Göteborg, Sweden*

Complete contact information is available at: https://pubs.acs.org/10.1021/acs.jpcc.4c00554


### Notes

The authors declare no competing financial interest.

## ■ ACKNOWLEDGMENTS

We acknowledge financial support from the Swedish Energy Agency (47110-1). The Competence Centre for Catalysis (KCK) is hosted by Chalmers University of Technology and financially supported by the Swedish Energy Agency (52689-1) and the member companies Johnson Matthey, Perstorp, Powercell, Preem, Scania CV, Umicore and Volvo Group. The calculations were performed at PDC (Stockholm) through a NAISS grant.

## ■ REFERENCES

(1) Commission proposes new Euro 7 standards to reduce pollutant emissions from vehicles and improve air quality. https://ec.europa.eu/commission/presscorner/detail/en/ip_22_6495web/(accessed March 11, 2024).

(2) Nova, I.; Tronconi, E. *Urea-SCR Technology for DeNO$_x$ After Treatment of Diesel Exhausts*; Springer Science+Business Media: New York, 2014.

(3) Schmieg, S. J.; Oh, S. H.; Kim, C. H.; Brown, D. B.; Lee, J. H.; Peden, C. H.; Kim, D. H. Thermal Durability of Cu-CHA $NH_3$-SCR Catalysts for Diesel $NO_x$ Reduction. *Catal. Today* **2012**, *184*, 252−261.

(4) Xin, Y.; Li, Q.; Zhang, Z. Zeolitic Materials for DeNO$_x$ Selective Catalytic Reduction. *ChemCatChem* **2018**, *10*, 29−41.

(5) Colombo, M.; Nova, I.; Tronconi, E. A Comparative Study of the $NH_3$-SCR Reactions over a Cu-Zeolite and a Fe-Zeolite Catalyst. *Catal. Today* **2010**, *151*, 223−230.

(6) Shan, Y.; Shi, X.; He, G.; Liu, K.; Yan, Z.; Yu, Y.; He, H. Effects of $NO_2$ Addition on the $NH_3$-SCR over Small-Pore Cu-SSZ-13 Zeolites with Varying Cu Loadings. *J. Phys. Chem. C* **2018**, *122*, 25948−25953.

(7) Gao, F.; Walter, E. D.; Kollar, M.; Wang, Y.; Szanyi, J.; Peden, C. H. Understanding Ammonia Selective Catalytic Reduction Kinetics over Cu/SSZ-13 from Motion of the Cu Ions. *J. Catal.* **2014**, *319*, 1−14.

(8) Fahami, A. R.; Günter, T.; Doronkin, D. E.; Casapu, M.; Zengel, D.; Vuong, T. H.; Simon, M.; Breher, F.; Kucherov, A. V.; Brückner, A.; et al. The Dynamic Nature of Cu Sites in Cu-SSZ-13 and the Origin of the Seagull $NO_x$ Conversion Profile during $NH_3$-SCR. *React. Chem. Eng.* **2019**, *4*, 1000−1018.

(9) Günter, T.; Pesek, J.; Schäfer, K.; Bertótiné Abai, A.; Casapu, M.; Deutschmann, O.; Grunwaldt, J. D. Cu-SSZ-13 as Pre-Turbine $NO_x$-Removal-Catalyst: Impact of Pressure and Catalyst Poisons. *Appl. Catal., B* **2016**, *198*, 548−557.

(10) Selleri, T.; Ruggeri, M. P.; Nova, I.; Tronconi, E. The Low Temperature Interaction of NO + $O_2$ with a Commercial Cu-CHA Catalyst: A Chemical Trapping Study. *Top. Catal.* **2016**, *59*, 678−685.

(11) Torp, T. K.; Hansen, B. B.; Vennestrøm, P. N. R.; Janssens, T. V. W.; Jensen, A. D. Modeling and Optimization of Multi-functional

Ammonia Slip Catalysts for Diesel Exhaust Aftertreatment. *Emiss. Control Sci. Technol.* **2021**, *7*, 7−25.
(12) Clark, A. H.; Nuguid, R. J. G.; Steiger, P.; Marberger, A.; Petrov, A. W.; Ferri, D.; Nachtegaal, M.; Kröcher, O. Selective Catalytic Reduction of NO with $NH_3$ on Cu-SSZ-13: Deciphering the Low and High-Temperature Rate-Limiting Steps by Transient XAS Experiments. *ChemCatChem* **2020**, *12*, 1429−1435.
(13) Feng, Y.; Janssens, T. V. W.; Vennestrøm, P. N. R.; Jansson, J.; Skoglundh, M.; Grönbeck, H. The Role of $H^+$- and $Cu^+$-Sites for $N_2O$ Formation during $NH_3$-SCR over Cu-CHA. *J. Phys. Chem. C* **2021**, *125*, 4595−4601.
(14) Feng, Y.; Wang, X.; Janssens, T. V. W.; Vennestrøm, P. N. R.; Jansson, J.; Skoglundh, M.; Grönbeck, H. First-Principles Microkinetic Model for Low-Temperature $NH_3$-Assisted Selective Catalytic Reduction of NO over Cu-CHA. *ACS Catal.* **2021**, *11*, 14395−14407.
(15) Bates, S. A.; Verma, A. A.; Paolucci, C.; Parekh, A. A.; Anggara, T.; Yezerets, A.; Schneider, W. F.; Miller, J. T.; Delgass, W. N.; Ribeiro, F. H. Identification of the Active Cu Site in Standard Selective Catalytic Reduction with Ammonia on Cu-SSZ-13. *J. Catal.* **2014**, *312*, 87−97.
(16) Gao, F.; Mei, D.; Wang, Y.; Szanyi, J.; Peden, C. H. Selective Catalytic Reduction over Cu/SSZ-13: Linking Homo- and Heterogeneous Catalysis. *J. Am. Chem. Soc.* **2017**, *139*, 4935−4942.
(17) Usberti, N.; Gramigni, F.; Nasello, N. D.; Iacobone, U.; Selleri, T.; Hu, W.; Liu, S.; Gao, X.; Nova, I.; Tronconi, E. An Experimental and Modelling Study of the Reactivity of Adsorbed $NH_3$ in the Low Temperature $NH_3$-SCR Reduction Half-Cycle over a Cu-CHA Catalyst. *Appl. Catal., B* **2020**, *279*, 119397.
(18) Shwan, S.; Skoglundh, M.; Lundegaard, L. F.; Tiruvalam, R. R.; Janssens, T. V. W.; Carlsson, A.; Vennestrøm, P. N. Solid-State Ion-Exchange of Copper into Zeolites Facilitated by Ammonia at Low Temperature. *ACS Catal.* **2015**, *5*, 16−19.
(19) Negri, C.; Borfecchia, E.; Cutini, M.; Lomachenko, K. A.; Janssens, T. V. W.; Berlier, G.; Bordiga, S. Evidence of Mixed-Ligand Complexes in Cu-CHA by Reaction of Cu Nitrates with $NO/NH_3$ at Low Temperature. *ChemCatChem* **2019**, *11*, 3828−3838.
(20) Paolucci, C.; Khurana, I.; Parekh, A. A.; Li, S.; Shih, A. J.; Li, H.; Di Iorio, J. R.; Albarracin-Caballero, J. D.; Yezerets, A.; Miller, J. T.; et al. Dynamic Multinuclear Sites Formed by Mobilized Copper Ions in $NO_x$ Selective Catalytic Reduction. *Science* **2017**, *357*, 898−903.
(21) Chen, L.; Janssens, T. V. W.; Vennestrøm, P. N. R.; Jansson, J.; Skoglundh, M.; Grönbeck, H. A Complete Multisite Reaction Mechanism for Low-Temperature $NH_3$-SCR over Cu-CHA. *ACS Catal.* **2020**, *10*, 5646−5656.
(22) Paolucci, C.; Parekh, A. A.; Khurana, I.; Di Iorio, J. R.; Li, H.; Albarracin Caballero, J. D.; Shih, A. J.; Anggara, T.; Delgass, W. N.; Miller, J. T.; et al. Catalysis in a Cage: Condition-Dependent Speciation and Dynamics of Exchanged Cu Cations in SSZ-13 Zeolites. *J. Am. Chem. Soc.* **2016**, *138*, 6028−6048.
(23) Paolucci, C.; Di Iorio, J. R.; Schneider, W. F.; Gounder, R. Solvation and Mobilization of Copper Active Sites in Zeolites by Ammonia: Consequences for the Catalytic Reduction of Nitrogen Oxides. *Acc. Chem. Res.* **2020**, *53*, 1881−1892.
(24) Liu, C.; Yasumura, S.; Toyao, T.; Maeno, Z.; Shimizu, K.-i. Mechanism of Standard $NH_3$-SCR over Cu-CHA via $NO^+$ and HONO Intermediates. *J. Phys. Chem. C* **2022**, *126*, 11594−11601.
(25) Chen, L.; Janssens, T. V. W.; Grönbeck, H. A Comparative Test of Different Density Functionals for Calculations of $NH_3$-SCR over Cu-Chabazite. *Phys. Chem. Chem. Phys.* **2019**, *21*, 10923−10930.
(26) Lomachenko, K.; Borfecchia, E.; Negri, C.; Berlier, G.; Lamberti, C.; Beato, P.; Falsig, H.; Bordiga, S. The Cu-CHA $deNO_x$ Catalyst in Action: Temperature-Dependent $NH_3$-Assisted Selective Catalytic Reduction Monitored by Operando XAS and XES. *J. Am. Chem. Soc.* **2016**, *138*, 12025−12028.
(27) Martini, A.; Borfecchia, E.; Lomachenko, K. A.; Pankin, I. A.; Negri, C.; Berlier, G.; Beato, P.; Falsig, H.; Bordiga, S.; Lamberti, C. Composition-Driven Cu-Speciation and Reducibility in Cu-CHA Zeolite Catalysts: A Multivariate XAS/FTIR Approach to Complexity. *Chem. Sci.* **2017**, *8*, 6836−6851.
(28) Chen, L.; Falsig, H.; Janssens, T. V. W.; Grönbeck, H. Activation of oxygen on $(NH_3-Cu-NH_3)^+$ in $NH_3$-SCR over Cu-CHA. *J. Catal.* **2018**, *358*, 179−186.
(29) Beale, A. M.; Gao, F.; Lezcano-Gonzalez, I.; Peden, C. H.; Szanyi, J. Recent Advances in Automotive Catalysis for $NO_x$ Emission Control by Small-Pore Microporous Materials. *Chem. Soc. Rev.* **2015**, *44*, 7371−7405.
(30) Janssens, T. V.; Falsig, H.; Lundegaard, L. F.; Vennestrøm, P. N. R.; Rasmussen, S. B.; Moses, P. G.; Giordanino, F.; Borfecchia, E.; Lomachenko, K. A.; Lamberti, C.; Bordiga, S.; et al. A Consistent Reaction Scheme for the Selective Catalytic Reduction of Nitrogen Oxides with Ammonia. *ACS Catal.* **2015**, *5*, 2832−2845.
(31) Gao, F.; Kwak, J. H.; Szanyi, J.; Peden, C. H. Current Understanding of Cu-Exchanged Chabazite Molecular Sieves for Use as Commercial Diesel Engine $DeNO_x$ Catalysts. *Top. Catal.* **2013**, *56*, 1441−1459.
(32) Borfecchia, E.; Lomachenko, K. A.; Giordanino, F.; Falsig, H.; Beato, P.; Soldatov, A. V.; Bordiga, S.; Lamberti, C. Revisiting the Nature of Cu Sites in the Activated Cu-SSZ-13 Catalyst for SCR Reaction. *Chem. Sci.* **2015**, *6*, 548−563.
(33) Kresse, G.; Hafner, J. Ab Initio Molecular Dynamics for Open-Shell Transition Metals. *Phys. Rev. B: Condens. Matter Mater. Phys.* **1993**, *48*, 13115−13118.
(34) Kresse, G.; Hafner, J. Ab Initio Molecular-Dynamics Simulation of the Liquid-Metalamorphous-Semiconductor Transition in Germanium. *Phys. Rev. B: Condens. Matter Mater. Phys.* **1994**, *49*, 14251−14269.
(35) Kresse, G.; Furthmüller, J. Efficient Iterative Schemes for Ab Initio Total-Energy Calculations Using a Plane-Wave Basis Set. *Phys. Rev. B: Condens. Matter Mater. Phys.* **1996**, *54*, 11169−11186.
(36) Kresse, G.; Furthmüller, J. Efficiency of Ab-Initio Total Energy Calculations for Metals and Semiconductors using a Plane-Wave Basis Set. *Comput. Mater. Sci.* **1996**, *6*, 15−50.
(37) Blöchl, P. E. Projector Augmented-Wave Method. *Phys. Rev. B: Condens. Matter Mater. Phys.* **1994**, *50*, 17953−17979.
(38) Kresse, G.; Joubert, D. From Ultrasoft Pseudopotentials to the Projector Augmented-Wave Method. *Phys. Rev. B: Condens. Matter Mater. Phys.* **1999**, *59*, 1758−1775.
(39) Perdew, J. P.; Burke, K.; Ernzerhof, M. Generalized Gradient Approximation Made Simple. *Phys. Rev. Lett.* **1996**, *77*, 3865−3868.
(40) Rivero, P.; Loschen, C.; Moreira, I. D. P. R.; Illas, F. Performance of Plane-Wave-Based LDA+U and GGA+U Approaches to Describe Magnetic Coupling in Molecular Systems. *J. Comput. Chem.* **2009**, *30*, 2316−2326.
(41) Isseroff, L. Y.; Carter, E. A. Importance of Reference Hamiltonians Containing Exact Exchange for Accurate One-Shot GW Calculations of $Cu_2O$. *Phys. Rev. B: Condens. Matter Mater. Phys.* **2012**, *85*, 235142.
(42) Grimme, S.; Antony, J.; Ehrlich, S.; Krieg, H. A Consistent and Accurate Ab Initio Parametrization of Density Functional Dispersion Correction (DFT-D) for the 94 Elements H-Pu. *J. Chem. Phys.* **2010**, *132*, 154104.
(43) Grimme, S.; Ehrlich, S.; Goerigk, L. Effect of the Damping Function in Dispersion Corrected Density Functional Theory. *J. Comput. Chem.* **2011**, *32*, 1456−1465.
(44) Mills, G.; Jónsson, H.; Schenter, G. K. Reversible Work Transition State Theory: Application to Dissociative Adsorption of Hydrogen. *Surf. Sci.* **1995**, *324*, 305−337.
(45) Henkelman, G.; Jónsson, H. Improved Tangent Estimate in the Nudged Elastic Band Method for Finding Minimum Energy Paths and Saddle Points. *J. Chem. Phys.* **2000**, *113*, 9978−9985.
(46) Gao, F.; Washton, N.; Wang, Y.; Kollár, M.; Szanyi, J.; Peden, C. Effects of Si/Al Ratio on Cu/SSZ-13 $NH_3$-SCR Catalysts: Implications for the Active Cu Species and the Roles of Brønsted Acidity. *J. Catal.* **2015**, *331*, 25−38.
(47) Chorkendorff, I.; Niemantsverdriet, J. W. *Concepts of Modern Catalysis and Kinetics*; John Wiley & Sons, 2017, p 109.


https://doi.org/10.1021/acs.jpcc.4c00554
J. Phys. Chem. C 2024, 128, 6689−6701

(48) Feng, Y. *Reaction Kinetics of $NH_3$-SCR over Cu-CHA from First Principles; licentiate thesis*; Chalmers University of Technology, 2021.
(49) Nielsen, D.; Gao, Q.; Janssens, T. V. W.; Vennestrom, P. N. R.; Mossin, S. Cu-Speciation in Dehydrated CHA Zeolites Studied by $H_2$-TPR and In Situ EPR. *J. Phys. Chem. C* **2023**, *127*, 12995−13004.
(50) Hu, W.; Gramigni, F.; Nasello, N. D.; Usberti, N.; Iacobone, U.; Liu, S.; Nova, I.; Gao, X.; Tronconi, E. Dynamic Binuclear $Cu^{II}$ Sites in the Reduction Half-Cycle of Low-Temperature $NH_3$-SCR over Cu-CHA Catalysts. *ACS Catal.* **2022**, *12*, 5263−5274.
(51) Marberger, A.; Petrov, A. W.; Steiger, P.; Elsener, M.; Kröcher, O.; Nachtegaal, M.; Ferri, D. Time-Resolved Copper Speciation during Selective Catalytic Reduction of NO on Cu-SSZ-13. *Nat. Catal.* **2018**, *1*, 221−227.
(52) Borfecchia, E.; Negri, C.; Lomachenko, K. A.; Lamberti, C.; Janssens, T. V. W.; Berlier, G. Temperature-Dependent Dynamics of $NH_3$-Derived Cu Species in the Cu-CHA SCR Catalyst. *React. Chem. Eng.* **2019**, *4*, 1067−1080.
(53) Wang, X.; Chen, L.; Vennestrøm, P. N. R.; Janssens, T. V. W.; Jansson, J.; Grönbeck, H.; Skoglundh, M. Direct Measurement of Enthalpy and Entropy Changes in $NH_3$ Promoted $O_2$ Activation over Cu-CHA at Low Temperature. *ChemCatChem* **2021**, *13*, 2577−2582.
(54) Zhang, D.; Yang, R. T. $N_2O$ Formation Pathways over Zeolite-Supported Cu and Fe Catalysts in $NH_3$-SCR. *Energy Fuels* **2018**, *32*, 2170−2182.
(55) Yao, D.; Liu, B.; Wu, F.; Li, Y.; Hu, X.; Jin, W.; Wang, X. $N_2O$ Formation Mechanism During Low-Temperature $NH_3$-SCR over Cu-SSZ-13 Catalysts with Different Cu Loadings. *Ind. Eng. Chem. Res.* **2021**, *60*, 10083−10093.
(56) Gao, F.; Walter, E. D.; Karp, E. M.; Luo, J.; Tonkyn, R. G.; Kwak, J. H.; Szanyi, J.; Peden, C. H. Structure-Activity Relationships in $NH_3$-SCR over Cu-SSZ-13 as Probed by Reaction Kinetics and EPR Studies. *J. Catal.* **2013**, *300*, 20−29.
(57) Liu, C.; Malta, G.; Kubota, H.; Toyao, T.; Maeno, Z.; Shimizu, K.-i. Mechanism of $NH_3$−Selective Catalytic Reduction (SCR) of $NO/NO_2$ (Fast SCR) over Cu-CHA Zeolites Studied by In Situ/Operando Infrared Spectroscopy and Density Functional Theory. *J. Phys. Chem. C* **2021**, *125*, 21975−21987.
(58) Hu, W.; Iacobone, U.; Gramigni, F.; Zhang, Y.; Wang, X.; Liu, S.; Zheng, C.; Nova, I.; Gao, X.; Tronconi, E. Unraveling the Hydrolysis of $Z_2Cu^{2+}$ to $ZCu^{2+}(OH)^-$ and Its Consequences for the Low-Temperature Selective Catalytic Reduction of NO on Cu-CHA Catalysts. *ACS Catal.* **2021**, *11*, 11616−11625.
(59) Campbell, C. T. Future Directions and Industrial Perspectives Micro- and Macro-Kinetics: Their Relationship in Heterogeneous Catalysis. *Top. Catal.* **1994**, *1*, 353−366.
(60) Ruggeri, M. P.; Nova, I.; Tronconi, E. Experimental Study of the NO Oxidation to $NO_2$ over Metal Promoted Zeolites Aimed at the Identification of the Standard SCR Rate Determining Step. *Top. Catal.* **2013**, *56*, 109−113.
(61) Liu, C.; Malta, G.; Kubota, H.; Kon, K.; Toyao, T.; Maeno, Z.; Shimizu, K. i. In Situ/Operando IR and Theoretical Studies on the Mechanism of $NH_3$-SCR of $NO/NO_2$ over H-CHA Zeolites. *J. Phys. Chem. C* **2021**, *125*, 13889−13899.
(62) Grossale, A.; Nova, I.; Tronconi, E.; Chatterjee, D.; Weibel, M. $NH_3$-$NO/NO_2$ SCR for Diesel Exhausts Aftertreatment: Reactivity, Mechanism and Kinetic Modelling of Commercial Fe- and Cu-Promoted Zeolite Catalysts. *Top. Catal.* **2009**, *52*, 1837−1841.
(63) Chen, L.; Falsig, H.; Janssens, T. V. W.; Jansson, J.; Skoglundh, M.; Grönbeck, H. Effect of Al-Distribution on Oxygen Activation over Cu-CHA. *Catal. Sci. Technol.* **2018**, *8*, 2131−2136.


https://doi.org/10.1021/acs.jpcc.4c00554
J. Phys. Chem. C 2024, 128, 6689−6701